An Investigation of Parametric Noise in Millimeter-Wave IMPATT Oscillators

ANDERS RYDBERG AND P. THOMAS LEWIN, MEMBER, IEEE

Abstract—**The IMPATT oscillator used as an LO source in a receiver has often been found to contribute a large amount of excess noise to the system (sometimes more than 40 dB compared to a klystron). Often the IMPATT noise has been referred to as avalanche noise, but theoretically this should only reduce the carrier-to-noise ratio by 10–15 dB when compared to a klystron.**

In the following paper, we show that the excess noise far from the carrier frequency (i.e., sideband noise) is much more dependent on parametric oscillations excited below the cutoff frequency of the mount than on avalanche noise.

By modifying the Hines equation for parametric stability, we have been able to investigate the parametric noise properties of realistic millimeter-wave IMPATT oscillators. Using theoretical waveguide models, we have investigated how the sideband noise depends on various mount configurations, avalanche currents, and IMPATT diodes. The calculated curves show good correlation with the measured noise at 4 GHz from the carrier.

It often has been found to be very difficult to completely reduce the parametric noise in avalanche oscillators. In these cases, the method of comparison between different mounts presented here for finding the diode-mount configuration which gives least parametric noise can be an aid in the construction of low-noise IMPATT oscillators.

I. Introduction

THE IMPATT DIODE exhibits negative resistance over a very large frequency range. It is therefore essential to provide the correct embedding impedance at frequencies far from the carrier region of the oscillator.

At high RF levels, even load impedances at frequencies far outside the negative resistance region have a profound effect on the stability of the oscillator. If the load impedance is not well controlled from very low frequencies (dc) up to the operating frequency, secondary effects such as bias oscillations and parametric instabilities can occur. These secondary effects create noise which modulates the carrier and reduces the signal-to-noise ratio of the IMPATT oscillator. This excess noise contribution often makes the IMPATT unsuitable as a mixer local oscillator in low-noise receiver systems.

The theory behind bias oscillations has been developed by Bracket [1]. He found that the source of bias oscillations is a low-frequency, RF-voltage-induced, negative resistance arising from (dc) rectification effects of the RF oscillation. The bias oscillations have been observed at frequencies up to several GHz for millimeter-wave IMPATT diodes [2].

The IMPATT diode has many similarities with the varactor diode. Hines [3] showed that the avalanche zone can be described as a linear capacitance shunted by a nonlinear inductance. Because of this nonlinear element, the IMPATT diode can be used for parametric amplification. This effect was investigated by Evans and Haddad [4] and Hines [3].

Supplying its own pump power (the fundamental oscillation), the IMPATT diode is therefore very prone to parametric oscillations. These oscillations can reduce the efficiency of the IMPATT oscillator and also contribute to the noise. In many cases, exceed noise of over 40 dB compared to a klystron has been observed at frequencies far away from the carrier (Gewartowski [5]). This result is confirmed in our study.

The first theoretical model of parametric instabilities was presented by Hines [3]. Using the model by Hines, Schroeder [6] developed a simplified theory of parametric instabilities in IMPATT circuits. This theory gives an insight into what embedding impedance is required at different frequencies to suppress parametric instabilities.

A special case of parametric instability, the so-called degenerate one, is when the parametric oscillation is generated at half the frequency of the pump signal. This case has been studied extensively by Peterson [7].

To our knowledge, publications to this date on parametric instabilities have been made using the Read diode model for the IMPATT device. In the Read model, the space-charge effects in the avalanche zone are neglected since the zone is assumed to be very thin. This model works very well in evaluating the small-signal impedance for low-frequency IMPATT devices [8]. However, the behavior of the small-signal impedance for millimeter-wave IMPATT diodes differs from diodes for lower (microwave) frequencies, since the effect of a finite avalanche width takes on greater importance at higher frequencies. The space-charge effects in the avalanche zone have a profound influence on the small-signal impedance at frequencies close to the so-called avalanche frequency, as defined by Gilden and Hines [8]. It is essential to have an accurate diode model at these frequencies since parametric instabilities usually occur in this range. An IMPATT diode de-

Manuscript received June 14, 1986; revised February 3, 1987. This work was supported in part by the Swedish Board for Technical Development.

A. Rydberg is with the Department of Radio and Space Science and the Onsala Space Observatory, Chalmers University of Technology, S-412 96 Göteborg, Sweden.

P. T. Lewin is with Ericsson Radio System AB, S-431 26 Mölndal, Sweden.

IEEE Log Number 8715003.

0018-9480/87/0700-0663$01.00 ©1987 IEEE

signed for around 100 GHz can still have a significant negative resistance at the avalanche frequency. In the Read model, the negative resistance becomes zero at the avalanche frequency, a consequence of neglecting the space-charge effect in the finite avalanche zone. Using the extended diode model developed by Kuo [9], we have modified the theory by Hines to be usable also for millimeter-wave diodes.

The probability of a parametric instability, which usually occurs below the cutoff frequency of the waveguide mount, is strongly dependent on the impedance seen by the diode. Therefore, it is essential to have waveguide models which give information as correct as possible on the behavior of the embedding impedance as a function of the waveguide dimensions, and the position of the diode and backshort. Such accurate waveguide models for different types of mounts have been developed by Williamson [10], [11].

Experimentally, we have found that normally the parametric instability is a mixture between the degenerate case and a case with two or several separate parametrically related frequencies. Low-frequency signals will be generated as mixing products between the parametric signals and appear as noisy sidebands around the pump frequency. We have experimentally found that the higher the calculated value of $|M_1|^2 \cdot |S_0(\omega_p/2)|^2$ as defined by Schroeder in [6], the more frequencies around $\omega_p/2$ will be susceptible to parametric instability. Thus, we have experimentally found a correlation between the variation of $|M_1|^2 \cdot |S_0(\omega_p/2)|^2$ and the sideband noise at the pump frequency. Several oscillators have been built to test this correlation and measurements of their noise performance show good agreement between calculations and experiments.

This paper provides a useful technique for predicting how the excessive sideband noise behaves as a function of the waveguide mount structure for different millimeter-wave IMPATT diodes and diode currents, resulting in some useful design rules on how to reduce the noise in IMPATT oscillators which are contaminated by or susceptible to parametric noise.

II. Review of the Criteria for Parametric Instability

For a parametric instability to be present in a nonlinear device, a "large-amplitude" pump signal is required. In the case of the IMPATT oscillator, the free-running oscillation provides the pump signal (ω_p) and the nonlinear inductance thus created the nonlinear element. If the load impedance of the IMPATT diode is not well controlled in the critical frequency range $\omega_p/4 \leqslant \omega \leqslant \omega_p/2$, the parametric instability can easily induce secondary effects such as spurious oscillation in combination with a high noise level.

Schroeder's investigation of parametric effects [6] resulted in two useful equations (see (1) and (2)), yielding criteria for the onset of parametric instabilities:

$$S_m = S(\omega_m) = 1 + \frac{\omega_m^2}{(\omega_a^2 - \omega_m^2)} \frac{Z_x(\omega_m) + \dfrac{1}{j\omega_m C_t}}{Z_x(\omega_m) + Z_{d\mathrm{READ}}(\omega_m)} \tag{1}$$

where

- ω_a avalanche resonance frequency of the IMPATT diode,
- C_t total depletion-layer capacitance of the diode,
- Z_x external impedance seen by the diode at the diode terminals,
- $Z_{d\mathrm{READ}}$ small-signal Read-model impedance derived by Gilden and Hines [8].

In order to avoid parametric instabilities, it is necessary that

$$|M_1|^2 \cdot S_0 \cdot S_{-1}^* \leqslant 1 \tag{2}$$

where M_1 is the ratio of the complex avalanche particle current at the pump frequency divided by the dc current. How to calculate the M_1 factor is described by Schroeder in [6]. S_0 is the stability factor for parametric instability at the frequency ω_0. Usually, $\omega_p/4 \leqslant \omega_0 \leqslant \omega_p/2$, where ω_p is the pump frequency. In the same way as S_0 is related to ω_0, S_{-1} is related to ω_{-1}, where $\omega_{-1} = \omega_p - \omega_0$. Equation (2) is called the stability equation, where the asterisk denotes complex conjugate.

The condition for the generation of parametric signals is that the imaginary part of $S_0 \cdot S_{-1}^*$ in (2) be zero and the real part be >1. At a sufficiently high pump power, $|M_1|$ will cause the left-hand side of (2) to become greater than 1; the circuitry will then start to generate a parametric signal pair. It should be noted that for the degenerate case (for which $\omega_0 = \omega_{-1} = \omega_p/2$), the stability factors S_0 and S_{-1} are identical and $S_0 \cdot S_{-1}^* = |S_0|^2$.

For unconditional stability at the subharmonic frequency $\omega_p/2$, it is then necessary to state the condition

$$|S_0(\omega_p/2)| \leqslant 1 \tag{3}$$

since the phase condition for instability is always satisfied at the subharmonic ($S_0 = S_{-1}$), and this suggests that the half pump frequency oscillation may be the most likely form of spurious oscillation. This was found to be the case in our experiment.

III. Stability Model for the Calculations

One means by which a signal around $\omega_p/2$ can be detected is by connecting a spectrum analyzer to the bias circuitry. The waveguide is normally cut off for this frequency. The bias port was connected to a bias tee, used for supplying the dc current to the diode. The ac port of the bias tee was connected to a coaxial waveguide transition attached to the harmonic mixer of the spectrum

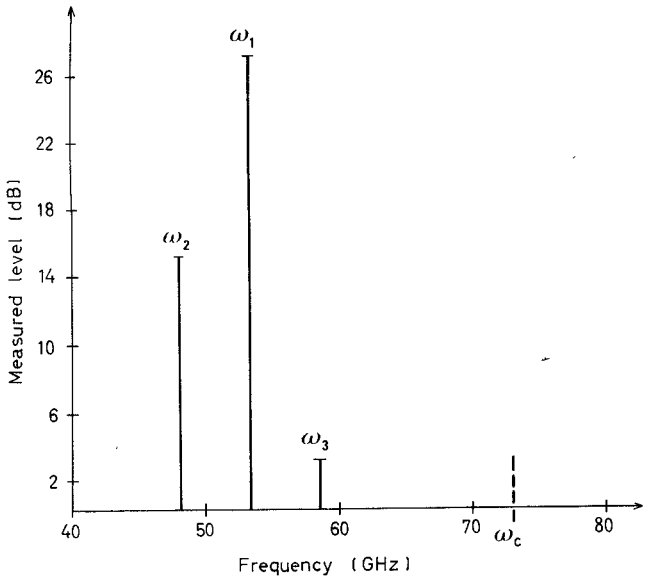

Fig. 1. Measured level and frequency of parametric oscillations below cutoff for an IMPATT diode post-mounted in WR-8 waveguide. Waveguide height is 0.4 mm and the diode is similar to diode A (see Table I). The carrier frequency for the oscillator ω_p was 106.8 GHz; ω_c = cutoff frequency for the WR-8 waveguide ($\omega_c = 73$ GHz). The following relation exists between the signals: $\omega_1 = \omega_p/2$; ω_2 and ω_3 are parametric oscillations: $\omega_p = \omega_2 + \omega_3$.

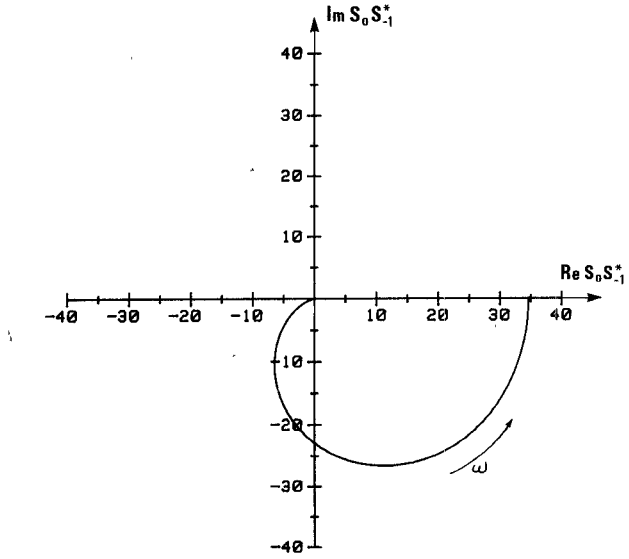

Fig. 2. Calculated $S_0 \cdot S_{-1}^*$ factor for $\omega_p/4 \leq \omega_0 \leq \omega_p/2$ at the pump frequency 106.8 GHz. The calculations are done for the same diode and mount as used in Fig. 1. The $|M_1|$ factor was found to be 0.61.

analyzer. With the spectrum analyzer we measured the frequency and the relative strength of the spurious oscillations which existed below the cutoff frequency for the waveguide mount (see Fig. 1). The bias tee in the system was designed for 1–18 GHz (SMA bias tee) and therefore introduced a strong mismatch at the measured frequencies ($\omega_p/2 = 50$–60 GHz). This and the fact that the bias circuitry itself is poorly matched to $\omega_p/2$ made it possible to get only a crude indication of the differences in the oscillation amplitude of the different oscillations. As expected, the oscillation at $\omega_p/2$, ω_1 in Fig. 1, was found to be the strongest. We also found an oscillation at ω_2 below ω_1 (Fig. 1). The oscillation at ω_2 was accompanied by an oscillation at ω_3 which satisfies the condition $\omega_p = \omega_2 + \omega_3$. The mixing products between the parametric oscillations are up-converted and appear as broad sidebands around the carrier. IMPATT devices have been found to work very efficiently as up-converters. For example Evans and Haddad [4] and Hines [3] found that the IMPATT device can show gain in up-conversion, especially for the lower sideband.

It was found that the carrier frequency ω_p was accompanied by signals at distances of $\omega_1 - \omega_2$ and $\omega_3 - \omega_2$ from the carrier. The sidebands were found to have a broad noise spectrum, covering several hundred megahertz at the frequencies for the mixing products $\omega_1 - \omega_2$ and $\omega_3 - \omega_2$. The mixing products varied in frequency, but were usually between 3 and 5 GHz from the carrier. At high noise levels, an almost flat noise spectrum was experienced. The low-frequency sidebands of ω_p were much stronger than the high-frequency sidebands. Sometimes the upper sideband could not be detected. This supports the use of only three frequencies, ω_0, ω_{-1}, and ω_p, in the calculation of the stability factors S_m in (1) (see [6]).

The measurements (see Section VI) show good correlation between the onset of excessive noise and the threshold for parametric instability at $\omega_p/2$, i.e., $|M_1|^2 \cdot |S_0(\omega_p/2)|^2 > 1$. We can therefore assume that the measured increase in noise is a result of up-conversion of noise generated by parametric oscillations. This assumption was found to be true since parametric oscillations at $\omega_p/2$ were observed in the measured oscillators. The existence of a signal at $\omega_p/2$, the degenerate parametric case, has been found to change the stability conditions for other frequencies around $\omega_p/2$ [12]. Unexpected variations in the impedance of the embedding network or the diode for frequencies near $\omega_p/2$ could also give rise to parametric signal pairs when the factor $|M_1|^2 \cdot |S_0(\omega_p/2)|^2$ is large. Thus, we found in the experiments that even though the calculated stability curve $S_0 \cdot S_{-1}^*$ for $\omega_p/4 < \omega_0 < \omega_p/2$ did not intersect the real axis above the value 1 (see Fig. 2), apart from the point $\omega_p/2$, parametric signal pairs were found accompanying the parametric oscillation at $\omega_p/2$ (see Fig. 1).

Experimental studies of nonlinear circuits similar to the IMPATT diode have shown that the noise level is proportional to the number of parametric signal pairs [13]. Thus, a correlation is to be expected between the variation of $|M_1|^2 \cdot |S_0(\omega_p/2)|^2$ and the variation of the sideband noise around the carrier arising from mixing products between the parametric oscillations. However the situation consisting of a mixture between the nondegenerative parametric case and the degenerative one is complicated to deal with theoretically.

It should be pointed out that only the correlation between the variation of the measured noise and the calculated value $|M_1|^2 \cdot |S_0(\omega_p/2)|^2$ is considered in this study.

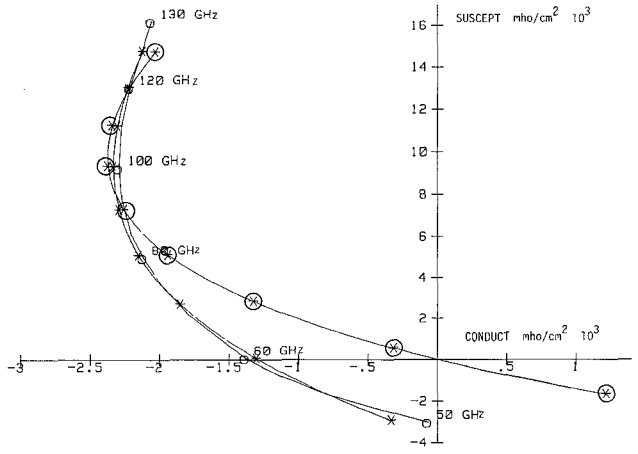

Fig. 3. Theoretically calculated admittance for a 94-GHz double-drift IMPATT diode compared to a published curve for such a device. The markings are at 10-GHz intervals. (○) = published curve [14]; (⊛) = Read-diode model [8]; (*) = diode model by Kuo [9].

IV. IMPATT Diode Modeling

We have used two different impedance equations in the calculation of Z_d, the Read diode model [8] (eq. 4 below) and the extended expression developed by Kuo [9] (eq. 5 below):

$$Z_{d\mathrm{READ}}(\omega) = \frac{x_d(1-(\sin\phi/\phi)) - \omega^2/\omega_a^2 + jx_d((1-\cos\phi)/\phi)}{j\omega C_t(1-\omega^2/\omega_a^2)} \quad (4)$$

$$Z_{d\mathrm{KUO}}(\omega) = \frac{1}{j\omega C_t} - \frac{\left(1-x_d+\frac{x_d}{j\omega\tau_d}(1-e^{-j\omega\tau d})\right)\left(1+j\omega R_a\frac{C_t}{(1-x_d)}\right)}{j\omega C_t\left(1+j\omega R_a\frac{C_t}{(1-x_d)}-\left(\frac{\omega}{\omega_a}\right)^2\right)} \quad (5)$$

where

- x_d fractional drift length,
- τ_d drift time,
- ϕ $\omega\cdot\tau_d$,
- ω_a avalanche frequency,
- R_a avalanche resistance,
- C_t total depletion-layer capacitance.

The Read diode model is based on the assumption of a very thin avalanche region, electrically equivalent to a nonlinear avalanche inductance in parallel with an avalanche capacitance C_a. The extended model by Kuo [9] is adapted for a finite avalanche zone by including an avalanche resistance R_a in series with the capacitance C_a.

Both models were matched (using the least mean square error criterion) to a published curve [14] of the admittance for a typical 94-GHz double drift IMPATT diode (see Fig. 3). The extended expression by Kuo [9] shows much better agreement with the published curve at the avalanche frequency ω_a because of the avalanche resistance R_a. It is essential to have an accurate impedance description of Z_d at these frequencies, since the parametric instabilities occur in this region.

TABLE I
Diode Descriptions

Diode	Capsule cap.(pF)	Bond. wire ind.(nH)	Diode diam. (μm)	Junction cap.(pF)[1]	V_{br} (V)	Designed for(GHz)[2]	Manufact.
A	0.1	0.03	45	0.85	14.2	94	Hughes
B	0.04	0.03	43	0.79	13.0	94	Hughes
C	0.1	0.03	37	0.66	12.8	94	Thomson

[1] at zero voltage.
[2] approximate frequency.

The diodes used in the experiments are listed in Table I. Diode A was designed for 94 GHz and has, according to the manufacturer, a diode diameter of around 45 μm [15]. The small differences in breakdown voltage for diodes B and C indicates that these devices were also optimized for a frequency close to 94 GHz [14]. Using diode A as a reference, we calculated the diode diameter for diode B and C by using the relationship between the junction capacitance and the diode diameter, assuming that the diodes all have the same doping profile as diode A. The published small-signal admittance curve for the 94-GHz diode, diode A, was calculated for a diode current density of 24 kA/cm^2, which with a diode diameter of 45 μm gave a diode current of 387 mA. Assuming (see above) that the other devices B and C were also designed for the same admittance curve, we derived the following diode currents: 341 mA for diode B and 270 mA for diode C. These currents I_c are used for calculating the avalanche resonance frequency at different diode dc currents for each diode using the following equation:

$$\omega_{na} = \omega_{ca}\sqrt{\frac{I_n}{I_c}} \quad (6)$$

where

- ω_{na} avalanche resonance frequency at the new dc current,
- ω_{ca} about 58 GHz (see Fig. 3),
- I_n new dc current,
- I_c for diode A: 387 mA, diode B: 341 mA, and diode C:270 mA (see above).

The new avalanche resonance frequency is then used in (5) to calculate the diode impedance at the new operating point.

Using the diode model by Kuo, the listed IMPATT diodes were matched separately (using the least mean square error criterion) to the curve of the admittance for the 94-GHz IMPATT diode. This means that all diode chips were given the same admittance versus frequency characteristic. The only difference in initial values between the diodes concerned the diode diameters, which were set fixed. From the matching, the parameters in (5) for each diode chip were derived.

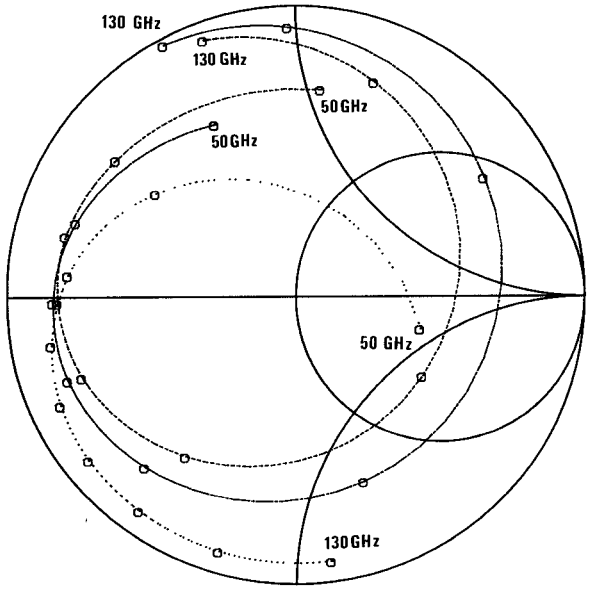

Fig. 4. Smith diagram showing the encapsulated diode impedance $(-Z_d)$ for the three different diodes: (---) = diode A (diode current = 280 mA); (· · ·) = diode B (diode current = 280 mA); (– · –) = diode C (diode current = 200 mA).

The calculated diode impedances $-Z_d$ for the encapsulated diodes are shown in the Smith diagram in Fig. 4.

Equation 1 is based on the Read diode model, $Z_{d\mathrm{READ}}(\omega)$. This means that the pole in (1) at $\omega = \omega_a$ is canceled by the similar pole in $Z_{d\mathrm{READ}}(\omega)$. By replacing $Z_{d\mathrm{READ}}(\omega)$ in (1) with $Z_{d\mathrm{KUO}}(\omega)$ (5), we see that the pole is no longer canceled by a pole in Z_d. This means that we have to rewrite (1) for the extended diode model. Following the calculations by Hines (3), we include a correction factor (see R factor) in (7) to accommodate for the diode model by Kuo in (5):

$$S_m = S(\omega_m) = 1 + \frac{\omega_m^2}{(R\cdot\omega_a^2 - \omega_m^2)} \frac{Z_x(\omega_m) + \dfrac{R}{j\omega_m C_a} + \dfrac{1}{j\omega_m C_d}}{Z_x(\omega_m) + Z_{d\mathrm{KUO}}(\omega_m)} \quad (7)$$

where

- ω_a avalanche resonance frequency of the IMPATT diode,
- C_t total depletion-layer capacitance of the diode,
- x_d fractional drift length,
- Z_x external impedance seen by the diode at the diode terminals,
- $Z_{d\mathrm{KUO}}$ Kuo equation for the small-signal impedance of the IMPATT,
- R $= 1 + j\omega R_a C_a$,
- R_a avalanche resistance [9],
- C_a avalanche capacitance, calculated as $C_t/(1 - x_d)$.

Equation (7) can easily be returned to its original expression, (1), the Read diode model, by putting $R_a = 0$ in the R factor.

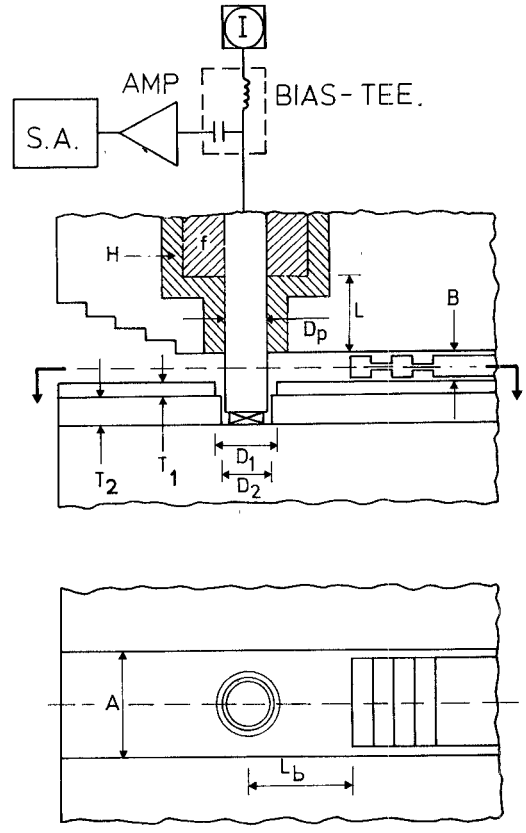

Fig. 5. Waveguide configuration and measurement system used in the experiments (for A, B, T_1, D_1, T_2, D_2, see Table II). A = waveguide width; B = waveguide height; T = thickness of diode spacer; D = diameter of hole in diode spacer; H = anodized aluminum cylinder; L = low-pass filter ($3\lambda/4$ at 100 GHz); f = ferrite material; D_p = post diameter (0.9 mm in all cases); L_b = backshort position; AMP = low-noise FET amplifier (200 K); I = bias current supply; S.A. = spectrum analyzer (Tektronix 492).

V. Waveguide Model

The IMPATT diode was postmounted in a reduced height waveguide (see Fig. 5). The bias circuit was loaded with ferrite material to ensure a high impedance at low frequencies and to prevent low frequency bias oscillations.

Using the waveguide models by Williamson [10], [11] on coaxial-waveguide and post waveguide mount structures, we calculated the embedding impedance for the circuit. The coaxial-waveguide models by Williamson have been investigated [16] for post diameters and coaxial aperture dimensions up to, respectively, 27 percent and 63 percent of the broad waveguide dimension where the theoretical results were found to lose accuracy. In our case, the same figures are, at the most, 35 percent and 59 percent, respectively. However, by careful judgement of how to compare different mounts and diodes, the calculation errors can be minimized (see discussion in Section VIII).

VI. Measurements and Calculations

The normal way to measure AM sideband noise from an oscillator is to use a noise-measurement setup at the carrier frequency [17]. This works well for close-to-carrier fre-

TABLE II
MOUNT CONFIGURATION

Mount	Waveg. dim.		Diode spacer dim.			
	A	B	T_1	T_2	D_1	D_2
1	2.54	0.4	0.1	0.4	1.5	1.2
2	2.54	0.4	0.1	0.25	1.5	1.2
3	2.54	0.4	-	-	-	-
4	2.54	0.7	-	-	-	-
5	2.03	0.4	0.4	-	1.2	-

Dimensions in mm.

quencies but is lacking in sensitivity for the frequencies we are interested in, which are between 3 and 5 GHz from the carrier. If there are discrete signals that give rise to the sidebands (see Section III and ω_1, ω_2, and ω_3 in Fig. 1), the mixing products of these signals (which were found to have a frequency of 3–5 GHz) should also be found on the bias line [18]. We found that the magnitude of the mixing products at 4 GHz on the bias line closely followed the behavior of the magnitude of the sideband noise at 4 GHz from the carrier. This is to be expected since the sideband noise and the noise on the bias line originate from the same parametric signals. The 4-GHz noise was measured using a bias tee, a low-noise FET amplifier ($T = 200$ K), and the 50 kHz–4.2 GHz frequency range of a spectrum analyzer (Tektronix 492), as shown in Fig. 5.

The reason for using 4 GHz as the measurement frequency is that this frequency is also used as the IF frequency in the radio astronomy system at the Onsala Space Observatory. It is therefore essential to have low noise at this frequency from the carrier if the IMPATT is going to be used as the local oscillator in these receivers.

Two different systems were used in the comparison between the 4 GHz noise on the bias line and the sideband noise at 4 GHz from the carrier. At high noise levels, a room-temperature Schottky-diode mixer followed by a spectrum analyzer was used. Due to lack of sensitivity, this system was replaced at low noise levels by a radiometer system similar to the system used in [19] using a cooled (20 K) Schottky-diode mixer. Results from the radiometer measurements are shown in Fig. 12. The increase of excess noise from 80 K to 200 K in Fig. 12 corresponded to a measured increase of 4 dB in the bias line noise.

The relative sideband noise level at 4 GHz from the carrier was measured for different waveguide mounts using the bias line (see Fig. 5 and Table II).

Using the waveguide models in Section V and the measured backshort positions (L_b in Fig. 5) for calculation of Z_x in (7), we calculated, using (5), (6), and (7), the value of $|M_1|^2 \cdot |S_0(\omega_p/2)|^2$ for mount 1 (Table II) and diode A (Table I) at three different diode currents: 240, 280, and 310 mA (see Fig. 6). The $|M_1|^2$ factor was calculated using the measured output power, as described by Schroeder in [6]. The experimentally measured noise is plotted in Fig. 6 and shows generally good agreement with the theoretical curves. The dotted line in the figure represents the level $|M_1|^2 \cdot |S_0(\omega_p/2)|^2 = 1$. At high noise levels, e.g., around 92 GHz (280-mA curve) and at 96 GHz (310-mA curve) in Fig. 1, an almost flat noise spectrum was experienced. A

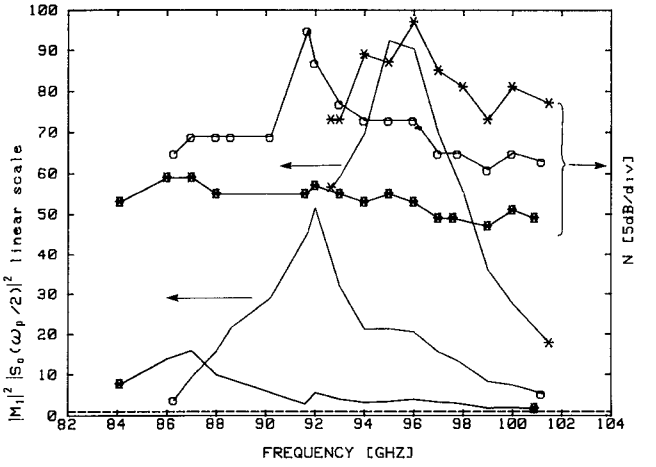

Fig. 6. Calculated $|M_1|^2 \cdot S_0 \cdot S^*_{-1}$ factor for $\omega_p/2$ ($|M_1|^2 \cdot |S_0(\omega_p/2)|^2$) and the measured relative level of the noise (N) at 4 GHz from the carrier as a function of ω_p using diode A in mount 1 at three diode currents: (⊛) = 240 mA; (○) = 280 mA; (*) = 310 mA.

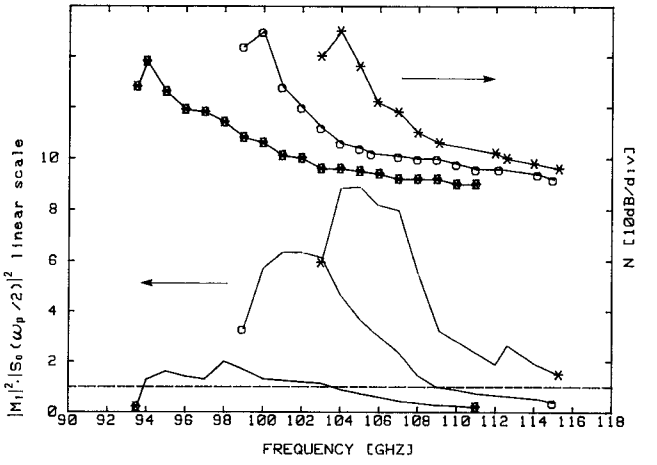

Fig. 7. Calculated $|M_1|^2 \cdot S_0 \cdot S^*_{-1}$ factor for $\omega_p/2$ ($|M_1|^2 \cdot |S_0(\omega_p/2)|^2$) and the measured relative level of the noise (N) at 4 GHz from the carrier as a function of ω_p using diode B in mount 2 at three diode currents: (⊛) = 200 mA; (○) = 240 mA; (*) = 280 mA.

flat noise spectrum at high noise levels was also experienced for the other oscillators.

The difference between the noise related to spurious oscillations (not parametrically related) and from parametric instabilities could be easily observed using an $E-H$ tuner at the output port of the IMPATT oscillator. The noise related to spurious oscillations was easily controlled by the tuner, while the influence on the parametric oscillations, which often occur below cutoff for the waveguide (especially for $\omega_p/2$ oscillations), was very small.

The noise from diode B mounted in a WR-10 waveguide (mount 2, Table II) was measured (see Fig. 7) at three different currents, namely 200, 240, and 280 mA. We see that the value of the avalanche current (diode current) plays an important role in the level of the parametric noise because of its influence on the avalanche frequency.

We found that the Kurokawa (coaxial-waveguide) circuit reduced the noise by 5 dB compared to a circuit consisting of only a reduced height waveguide (see Fig. 8).

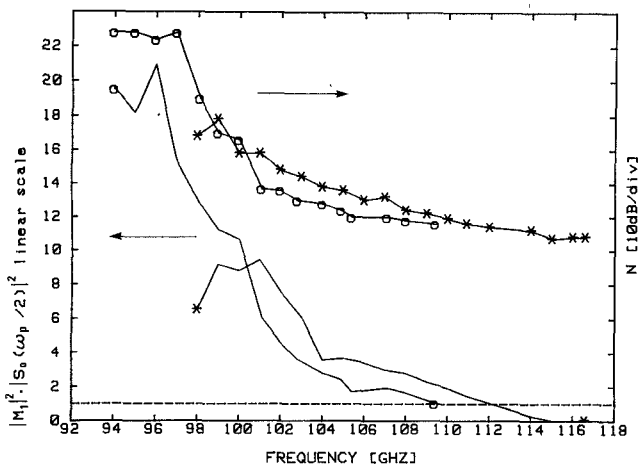

Fig. 8. Calculated $|M_1|^2 \cdot S_0 \cdot S^*_{-1}$ factor for $\omega_p/2$ ($|M_1|^2 \cdot |S_0(\omega_p/2)|^2$) and the measured relative level of the noise (N) at 4 GHz from the carrier as a function of ω_p using diode C in mount 3 and mount 2 (Kurokawa mount) at a diode current of 200 mA: (O) = mount 2; (*) = mount 3.

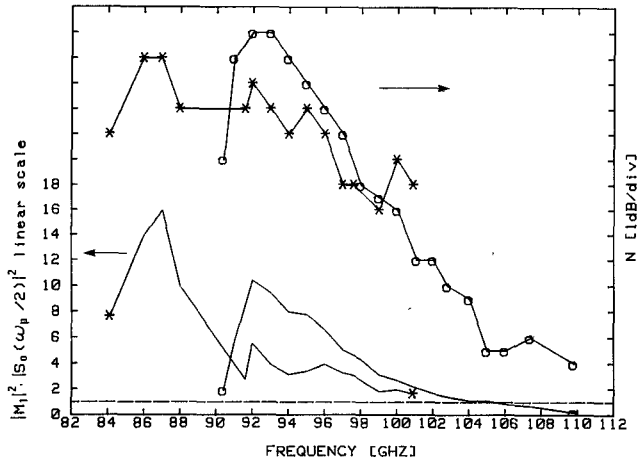

Fig. 9. Calculated $|M_1|^2 \cdot S_0 \cdot S^*_{-1}$ factor for $\omega_p/2$ ($|M_1|^2 \cdot |S_0(\omega_p/2)|^2$) and the measured relative level of the noise (N) at 4 GHz from the carrier as a function of ω_p using diode A in mount 1 and 2 at a diode current of 240 mA: (*) = mount 1; (O) = mount 2.

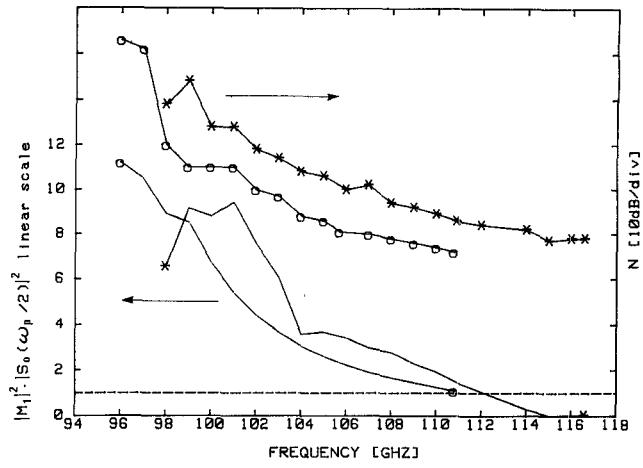

Fig. 10. Calculated $|M_1|^2 \cdot S_0 \cdot S^*_{-1}$ factor for $\omega_p/2$ ($|M_1|^2 \cdot |S_0(\omega_p/2)|^2$) and the measured relative level of the noise (N) at 4 GHz from the carrier as a function of ω_p using diode C in mount 3 and 4 at a diode current of 200 mA: (*) = mount 3; (O) = mount 4.

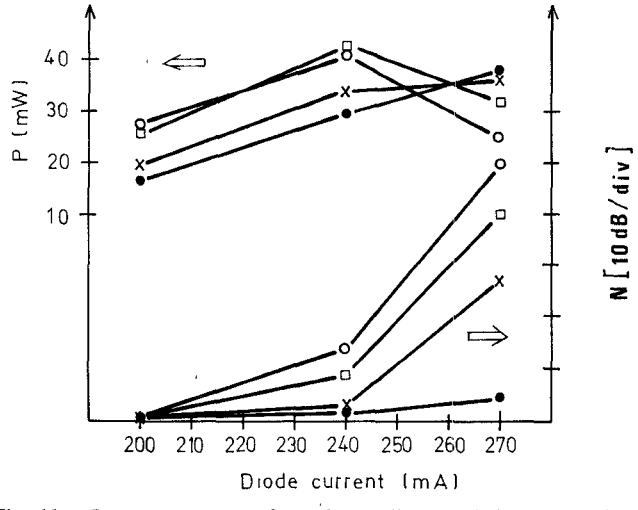

Fig. 11. Output power (P) from the oscillator and the measured relative level of the noise (N) at 4 GHz from the carrier as a function of the IMPATT diode current for diode B in mount 5 with the oscillator frequency as the parameter: (O) = 102 GHz; (□) = 103 GHz; (*) = 104 GHz; (·) = 105 GHz.

The output power for diode C was 4 percent higher for the frequency range 101–109 GHz using mount 3 than for mount 2.

The correlation between the length of the coaxial section ($T_1 + T_2$ in Fig. 5) in the Kurokawa circuit and the measured noise N is seen in Fig. 9. By increasing the length of the coaxial section, we increase the evanescent mode reactance at the diode plane, thereby reducing the $|S_0(\omega_p/2)|^2$ factor. This change in noise between the two circuits is predicted by the theory, as can be seen from the theoretical curves in Fig. 9. It can also be seen that the onset of excess noise is close to the frequency for the threshold of parametric instability. Mount 3 gave 30 percent more output power than mount 1 for the frequency range 92–101 GHz.

To investigate the influence of the waveguide height on the parametric noise, diode C was tested in mounts 3 and 4 at a diode current of 200 mA (see Fig. 10). About 18 percent more output power was achieved using mount 4 compared to mount 3 for the frequency range 101–108 GHz.

Using the measuring system in Fig. 5 (diode C, mount 5), we also measured the output power versus noise at different diode currents and oscillation frequencies (see Fig. 11). It can be seen that there is a correlation between low output power and high noise. This supports the conclusion made by others [7], [18] that the onset of subharmonic oscillation can severely limit the power output of an IMPATT oscillator or amplifier.

The noise temperature for a low-noise Schottky mixer system using an IMPATT oscillator (diode C, mount 3) as the LO source was measured as a function of the output power (see Fig. 12). The calculated $|M_1|^2 \cdot |S_0(\omega_p/2)|^2$ factor for different output powers is also shown in Fig. 12. Maximum output power was found to be close to 80 mW for diode C. It can be seen that if the noise at 4 GHz from the carrier was reduced by 10–20 dB, it would be possible

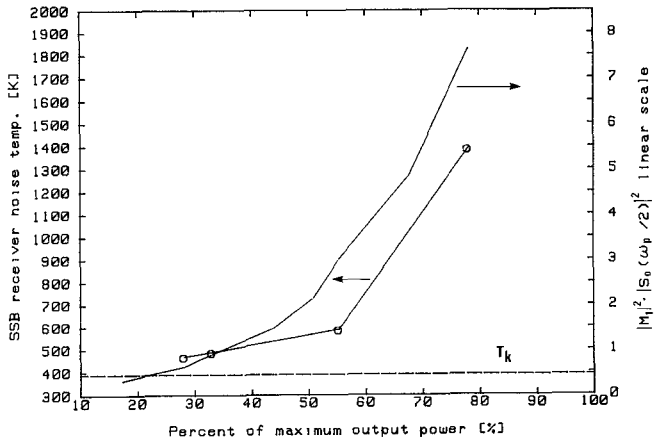

Fig. 12. Measured SSB receiver noise temperature at 115 GHz of a low-noise Schottky mixer system using an IMPATT oscillator at 111 GHz as the local oscillator (LO), plotted as function of percentage of maximum IMPATT output power. Here, 100-percent output power is equal to 80 mW. The noise temperature T_k using a klystron as the LO is shown for comparison. The calculated $|M_1|^2 \cdot S_0 \cdot S^*_{-1}$ factor for $\omega_p/2$ ($|M_1|^2 \cdot |S_0(\omega_p/2)|^2$) is also plotted in the diagram. Mount 3 was used in the experiment. The LO input power to the mixer was held constant.

to use an IMPATT oscillator for the LO in a low-noise Schottky receiver.

VII. Design Considerations

Testing different waveguide mounts, we found that the Kurokawa circuit is useful in suppressing the parametric sideband noise. The higher output power in this case also speaks in favour of this mount. The sideband noise was found to fall off as the length of the coaxial section increased. However, this is a choice between having maximum output power or minimum noise. Another consideration is the operating range, where an increased length of the coaxial section usually means a reduction in the maximum oscillation frequency for the oscillator, as can be seen in Fig. 9.

It was also found that an increase in the waveguide height reduced the measured noise. Thus, a Kurokawa structure with a full height waveguide might be a fruitful way of suppressing the noise.

The parametric noise is very sensitive to the frequency of the avalanche resonance. An important means of reducing the noise seems to be to push the avalanche resonance as low in frequency as possible, i.e., choosing a diode for a lower frequency while maintaining sufficient negative resistance at the pump frequency. The encapsulated diode can then be designed for maximum output at the pump frequency by optimizing the capsule parasitics, that is, the bonding wire inductance and the capsule capacitance.

Another important parameter is the magnitude of the avalanche current. There is a competition between having low sideband noise and high output power.

Under some circumstances, a high noise level is desirable, for example, in using IMPATT oscillators as noise sources.

VIII. Discussion and Conclusions

The accuracy in the calculation of $|M_1|^2 \cdot (S_0 \cdot S^*_{-1})$ is of course dependent on the accuracy of the waveguide model and the model for the IMPATT diodes. An error is introduced in the calculations by using the waveguide models [10], [11] (see Section V above) together with large post diameters. This error is at its largest when comparing two different waveguide structures, i.e., the normal reduced height waveguide structure and the Kurokawa structure (see Fig. 8). The influence from the error can be minimized by comparing the same types of waveguide structures (see Figs. 9 and 10).

Errors in the diode model can in the same way be reduced to a minimum by using the same operating point and diode for different oscillator mounts in comparing the calculated stability values $|M_1|^2 \cdot |S_0(\omega_p/2)|^2$ for the mounts.

We found in the experiments that the correlation between the measured noise and calculated stability factor $|M_1|^2 \cdot |S_0(\omega_p/2)|^2$ was best at low diode currents. This is to be expected since the first parametric instability at "low" diode currents occurs at $\omega_p/2$. By increasing the diode current, parametric instabilities will arise at other frequencies apart from $\omega_p/2$. A further increase in the avalanche current will create a state of chaos [13].

The spectrum of the pump signal for most oscillators tested above showed close resemblance to published curves for similar oscillators, even though the calculated $|M_1|^2 \cdot |S_0(\omega_p/2)|^2$ factors for the oscillators were found to be large. This suggests that a large amount of the excess noise generated in IMPATT oscillators has its cause in parametric instabilities.

Using the method described together with a large-signal diode model, it is possible to calculate the $|M_1|^2 \cdot |S_0(\omega_p/2)|^2$ factor and thereby evaluate the parametric noise behavior of different oscillator mounts.

Acknowledgment

The authors would like to thank Prof. E. Kollberg for continuous encouragement and support. They thank Dr. J. Ellder at the Onsala Space Observatory for his help in measuring the curve plotted in Fig. 12 and Dr. A. G. Williamson at the University of Auckland, New Zealand, for sending them his internal reports on post-waveguide structures. Thanks are due to the reviewers for their very helpful comments on this paper and to N. Whyborn and Dr. S. Withington for a critical reading of the manuscript.

References

[1] C. A. Bracket, "The elimination of tuning induced burnout and bias-circuit oscillations in IMPATT oscillators," *Bell Syst. Tech. J.*, vol. 52, pp. 271–306, 1973.

[2] Y. Hirachi, T. Nakagami, Y. Toyama, and Y. Fukukawa, "High-power 50 GHz double-drift region IMPATT oscillators with improved bias circuit for eliminating low frequency instabilities," *IEEE Trans. Microwave Theory Tech.*, vol. MTT-24, pp. 731–737, 1976.

[3] M. E. Hines, "Large signal noise frequency conversion, and parametric instabilities in IMPATT diode networks," *Proc. IEEE*, vol. 60, pp. 1524–1546, 1972.
[4] W. J. Evans and G. I. Haddad, "Frequency conversion in IMPATT diodes," *IEEE Trans. Electron Devices*, vol. ED-16, pp. 78–87, 1969.
[5] J. W. Gewartowski, "Progress with CW IMPATT diode circuits at microwave frequencies," *IEEE Trans. Microwave Theory Tech.*, vol. MTT-27, pp. 434–441, 1979.
[6] W. E. Schroeder, "Spurious parametric oscillations in IMPATT diode circuits," *Bell Syst. Tech. J.*, vol. 53, pp. 1187–1210, Sept. 1974.
[7] D. F. Peterson, "Circuit conditions to prevent second-harmonic power extraction in periodically driven IMPATT diode networks," *IEEE Trans. Microwave Theory Tech.*, pp. 784–790, 1974.
[8] M. Gilden, and M. E. Hines, "Electronic tuning effects in the Read microwave avalanche diode," *IEEE Trans. Electron Devices*, vol. ED-13, pp. 169–175, 1966.
[9] Y. L. Kuo, "Modelling of IMPATT diodes for circuit and noise analysis," presented at the IEEE Int. Symp. Circuits and Systems, Newton, MA, April 1975.
[10] A. G. Williamson, "Analysis and modelling of a single-post waveguide mounting structure," *Proc. Inst. Elec. Eng.*, vol. 129, pt. H, pp. 271–277, 1982.
[11] A. G. Williamson, "Analysis and modelling of a coaxial-line/rectangular-waveguide junction," *Proc. Inst. Elec. Eng.*, vol. 129, pt. H, pp. 262–270, 1982.
[12] D. Tang and G. I. Haddad, "Effects of the depletion-layer modulation on spurious oscillations in IMPATT diodes," *IEEE Trans. Microwave Theory Tech.*, vol. MTT-25, pp. 734–741, 1977.
[13] J. Testa, J. Perez, and C. Jeffris, "Evidence for universal chaotic behavior of a driven nonlinear oscillator," *Phys. Rev. Lett.* no. 11, pp. 714–717, 1982.
[14] H. J. Kuno, "IMPATT devices for generation of millimeter waves," in *Infrared and Millimeter Waves*, vol. 1. New York: Academic press, 1979, p. 60.
[15] H. J. Kuno and T. T. Fong, "Solid state mm-wave sources and combiners," *Microwave J.*, June 1979.
[16] A. G. Williamson, "Analysis of a coaxial line–rectangular waveguide circuit," School of Engineering Rep. No. 236, Department of Electrical Engineering, University of Auckland, New Zealand.
[17] J. G. Ondria, "A microwave system for measurements of AM and FM noise spectra," *IEEE Trans. Microwave Theory Tech.*, vol. MTT-16, pp. 767–781, 1968.
[18] K. P. Weller, D. L. English, and E. M. Nakaji, "High power *V*-band double drift IMPATT amplifier," in *Proc. IEEE Microwave Conf.* 1978, pp. 369–371.
[19] G. A. Ediss, N. J. Keen, and P. Zimmerman, "Comparison of AM noise from a klystron and an IMPATT oscillator at around 90 GHz," *IEEE Trans. Microwave Theory Tech.*, vol. MTT-30, pp. 2012–2013, 1982.

✠

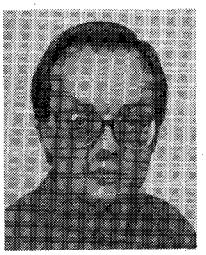

Anders Rydberg was born in Lund, Sweden, in 1952. He received the M.Sc. degree from Lund Institute of Technology in 1976.

He worked for two years at the National Defense Research Institute in Linköping with microwave technology, after which he joined the ELLEMTEL Company for one year. In 1986, he received the degree of Licentiate in Engineering from Chalmers University of Technology. He is presently working towards the Ph.D. degree in the area of millimeter-wave oscillators and multipliers.

✠

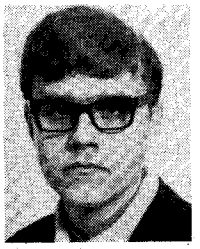

P. Thomas Lewin (M'85) was born in Uppsala, Sweden, in 1947. He received the civilingenjör (M.Sc) degree in electrical engineering in 1972 and the Ph.D. degree in 1978 from Chalmers University of Technology, Göteborg, Sweden.

In 1978, he joined Ericsson, Mölndal, Sweden, where he has been engaged in the development of solid-state microwave and millimeter-wave devices.